HHS Public Access

Author manuscript

Transl Stroke Res. Author manuscript; available in PMC 2024 April 01.

Published in final edited form as:

Transl Stroke Res. 2023 April ; 14(2): 238–249. doi:10.1007/s12975-022-01031-6.

Iron-induced hydrocephalus: the role of choroid plexus stromal macrophages

Chaoyi Bian[1,2,*], **Yingfeng Wan**[1,*], **Sravanthi Koduri**[1], **Ya Hua**[1], **Richard F. Keep**[1], **Guohua Xi**[1]

[1]Department of Neurosurgery, University of Michigan, Ann Arbor, Michigan, USA

[2]Department of Neurosurgery, Sir Run Run Shaw Hospital, Zhejiang University, Hangzhou, China

Abstract

Evidence indicates that erythrocyte-derived iron and inflammation both play a role in intraventricular hemorrhage-induced brain injury including hydrocephalus. Many immune-associated cells, primarily stromal macrophages, reside at the choroid plexus where they are involved in inflammatory responses and antigen presentation. However, whether intraventricular iron impacts those stromal cells is unknown. The aim of this study was to evaluate the relationship between choroid plexus stromal macrophages and iron-induced hydrocephalus in rats and the impact of minocycline and clodronate liposomes on those changes.

Aged (18-month-old) and young (3-month-old) male Fischer 344 rats were used to study choroid plexus stromal macrophages. Rats underwent intraventricular iron injection to induce hydrocephalus and treated with either minocycline, a microglia/macrophage inhibitor, or clodronate liposomes, a macrophage depleting agent. Ventricular volume was measured using magnetic resonance imaging and stromal macrophages were quantified by immunofluorescence staining. We found that stromal macrophages accounted for about 10% of the total choroid plexus cells with more in aged rats. In both aged and young rats, intraventricular iron injection resulted in hydrocephalus and increased stromal macrophage number. Minocycline or clodronate liposomes ameliorated iron-induced hydrocephalus and the increase in stromal macrophages.

In conclusion, stromal macrophages account for ~10% of all choroid plexus cells, with more in aged rats. Treatments targeting macrophages (minocycline and clodronate liposomes) are associated with reduced iron-induced hydrocephalus.

Keywords

Hydrocephalus; stromal macrophage; iron; minocycline; clodronate liposome

Correspondence: Guohua Xi, M.D., R5018 BSRB, University of Michigan, 109 Zina Pitcher Place, Ann Arbor, Michigan 48109-2200, Telephone: (734) 764-1207, Fax: (734) 763-7322, guohuaxi@umich.edu.

*Chaoyi Bian and Yingfeng Wan contributed equally to this study

Conflict of Interests: Chaoyi Bian, Yingfeng Wan, Sravanthi Koduri, Ya Hua, Richard F. Keep, and Guohua Xi declare no conflict of interests.

Competing interests: Guohua Xi is Deputy Editor-in-Chief of Translational Stroke Research.

Ethical approval: All institutional and national guidelines for the care and use of laboratory animals were followed.

Introduction

The choroid plexus is highly vascularized with a dense network of fenestrated capillaries surrounded by a monolayer of cuboidal epithelial cells with intervening stroma [1]. Cells and substances in blood can traverse the vascular endothelium and enter the stroma [2, 3] but entry into cerebrospinal fluid (CSF) is inhibited by the blood-cerebrospinal fluid barrier (BCSFB) at the epithelium [4, 5]. The choroid plexus is the primary site of CSF production. In the classic model, CSF normally flows through the ventricular system, but obstructed flow, limited CSF reabsorption or CSF overproduction can cause hydrocephalus [6].

The choroid plexus is also an important site in brain immune responses [1]. There are large numbers of OX-6 positive (+) cells. These are primarily macrophages with a small percentage attributable to other cell types, such as dendritic cells (DCs) [7]. Choroid plexus macrophages include both cells in the stroma and epiplexus (Kolmer) cells at the epithelial apical surface [1, 8]. The role of choroid plexus macrophages is still unclear but they are hypothesized to be involved in immune inflammatory responses and antigen presentation [9, 10]. In some pro-inflammatory conditions such as multiple sclerosis, choroid plexus macrophages are activated and increase in number [11]. However, more research is needed to further elucidate their roles.

Intraventricular hemorrhage (IVH) and associated hydrocephalus are major neurological issues in both neonates and adults [12]. In adults, IVH can follow both intracerebral and subarachnoid hemorrhage. Intracerebral hemorrhage is particularly a disease of the elderly and the occurrence of IVH and hydrocephalus is associated with worse outcomes [13-15]. While mechanisms of brain injury after cerebral hemorrhage are multifactorial, including a sudden increase in intracranial pressure, decreased cerebral blood flow and increased cerebral edema, evidence implicates iron and inflammation as potent mediators [15]. Iron is a major erythrocyte component and, after a cerebral hemorrhage, lysis of erythrocytes and hemoglobin degradation lead to iron release. Animal experiments indicate iron is important in IVH-induced neuronal damage and hydrocephalus [16, 17]. Our prior studies found lateral ventricle dilation and periventricular iron deposition in rat IVH and subarachnoid hemorrhage models [18-20] and intraventricular injection of iron itself caused hydrocephalus that was blocked by deferoxamine, an iron chelator [21, 22]. Whether iron might impact choroid plexus immune cells and whether this might contribute to hydrocephalus is unknown.

The current study examines choroid plexus histology in aged Fischer 344 (F344) rats to describe the normal morphological structure, distribution, and number of OX-6 (+) cells. Aged F344 rats also underwent intraventricular iron injection and were observed for OX-6 (+) cell activation and hydrocephalus development with MRI. Similar studies were carried out in young rats to examine the impact of aging. To potentially mitigate the effects of intraventricular iron injection, minocycline and clodronate liposomes were used.

Minocycline inhibits macrophages/microglia [23] and it is protective in multiple animal stroke models, including cerebral hemorrhage [24]. Our prior studies found it alleviated iron overload [25] and reduced macrophage activation [18] and it can reduce gliosis,

brain edema and hydrocephalus in some models of hydrocephalus [23, 26]. In addition, a recent study demonstrated that minocycline can protect against brain injury in a minipig ICH model, reducing lesion volume, ventricle enlargement and white matter injury [27]. Clodronate liposomes can induce macrophage depletion [28-30]. Polfliet et al. found that a single intraventricular injection of 50 μl of clodronate liposomes depleted perivascular and meningeal macrophages [31]. Based on that study, we hypothesized that intraventricular injection of clodronate liposomes will deplete choroid plexus macrophages.

Materials and Methods

Animal preparation and intraventricular injection

The University of Michigan Committee on the Use and Care of Animals approved the animal use protocols. A total of 28 male aged (18-month-old) F344 rats (National Institutes of Health, Bethesda, MD) and 32 male young (3-month-old) F344 rats (ENVIGO) were used. Animals were anesthetized with pentobarbital (50 mg/kg intraperitoneally) and body temperature maintained at 37.5°C with a heating pad. In a stereotactic frame (Kopf Instruments, Tujunga, CA), a cranial burr hole (1 mm) was drilled and a 26-gauge needle stereotactically inserted into the right lateral ventricle (coordinates: 0.6 mm posterior, 4.5 mm ventral, and 1.6 mm lateral to the bregma). A microinfusion pump (World Precision Instruments Inc., Sarasota, FL) was used for intraventricular injections (14 μl/min). The needle was left in place for an additional one minute after completion of the injection, the burr hole sealed with bone wax and the skin incision sutured closed.

Experimental groups

This study was subdivided into four parts with animals randomized into each group. First, normal aged F344 rats were euthanized and baseline specimens were collected (n=6). Second, aged F344 rats underwent intraventricular injection of saline (50 μl, n=6), $FeCl_3$ (2 mmol/L, 50 μl, n=8) or $FeCl_3$+minocycline (final concentration 2 mmol/L, 0.5 mmol/L respectively, 50 μl, n=8) into the right lateral ventricle at a rate of 14 μl/min. At 24 hours after injection, the rats underwent MRI scanning and were euthanized. Third, young F344 rats underwent saline intraventricular injection (50 μl, n=7), $FeCl_3$ (2 mmol/L, 50 μl, n=7) or $FeCl_3$+minocycline (final concentration 2 mmol/L, 0.5 mmol/L respectively, 50 μl, n=7) into the right lateral ventricle at a rate of 14 μl/min. At 24 hours after injection, the rats underwent MRI scanning and were euthanized. Finally, young F344 rats underwent intraventricular injection of $FeCl_3$+clodronate liposome (final concentration 2 mmol/L, 3.5 g/L respectively, 50 μl, n=6) or $FeCl_3$+control liposome (final concentration 2 mmol/L, 3.5 g/L respectively, 50 μl, n=6) into the right lateral ventricle. At 24 hours after injection, the rats underwent MRI imaging and were euthanized. One rat in the $FeCl_3$+clodronate liposome group was excluded due to the development of IVH and large periventricular hematoma following injection.

MRI scanning and ventricle volume measurement

For MRI scanning, rats were anesthetized with 2% isoflurane. MRI was obtained in a 7.0-T Varian MR scanner (Varian Inc.). The imaging protocol for all rats included a T2 fast spin-echo sequence (TR/TE=4000/60 msec). The field of view was 35 mm × 35 mm, and

the matrix was 256 mm×128 mm. Twenty-five coronal slices (0.5 mm thick) were acquired to cover the lateral ventricle system. Ventricular volumes were calculated as previously validated [16, 19]. Briefly, bilateral lateral ventricles were outlined and the area on each slice was measured. Ventricular volume was calculated by multiplying the ventricular area by section thickness. A blinded observer performed the image analyses using Image J.

Immunohistochemistry and immunofluorescence staining

Rats euthanized with pentobarbital (100 mg/kg intraperitoneal) underwent transcardiac perfusion with 4% paraformaldehyde in 0.1 mol/L phosphate-buffered saline (pH 7.4). The brains were stored in 4% paraformaldehyde for one day followed by immersion in 30% sucrose for 3 days at 4°C. They were then embedded in optimal cutting temperature compound (Sakura Finetek USA) prior to sectioning (18-μm) on a cryostat. Immunofluorescence studies were performed as previously described[32]. Briefly, primary antibodies were added and incubated overnight at 4°C followed by a phosphate buffered saline wash and incubation at room temperature for 2 hours with secondary antibodies. Primary antibodies were monoclonal mouse anti-OX-6 (1:200 dilution; BIO-RAD), polyclonal goat anti-Iba-1 (1:200 dilution; Abcam), and monoclonal rabbit anti-beta catenin (1:200 dilution; Abcam). Secondary antibodies were Alexa Fluor 488 donkey anti-goat IgG (1:500, Invitrogen), Alexa Fluor 594 donkey anti-mouse IgG (1:500, Invitrogen) and Alexa Fluor 488 donkey anti-rabbit IgG (1:500, Invitrogen). Fluoroshield™ with DAPI (F6057) was used for nuclear labeling.

Cell Counts

Immune-associated cells were assessed on high-power images (x40 magnification) taken by a digital camera. The brain section (~0.4 mm posterior to the bregma) with two choroid plexuses in bilateral lateral ventricles was chosen to count cells. The percentage of immune-associated cells was calculated as a percentage of total choroid plexus cell number. Choroid plexus cells from bilateral lateral ventricles were counted. Cell counts were performed using Image J. All measurements were repeated three times by a blinded observer and the mean value was used.

Statistical Analysis

Values are given as means ± standard deviation (SD). Student t-test or one-way ANOVA with a Tukey's multiple comparisons test were used to analyze the data. Differences were considered significant at $p<0.05$.

Results

OX-6 (+) cells, the majority of which are macrophages, are primarily located in the choroid plexus stroma

Initial experiments were geared towards describing the baseline state of OX-6 (+) cells in the choroid plexus. This was achieved by immunofluorescence double-staining of OX-6 and beta-catenin in normal aged F344 rats. Most OX-6 (+) cells were found to be located between the choroid plexus vasculature and epithelium, a region that is described as the

choroid plexus stroma. The cellular morphology of these OX-6 (+) cells was variable and included elongated, dendriform or amoeboid appearances (Figure 1A).

OX-6 (+) cells in the choroid plexus were further sub-classified by immunofluorescence double-staining for OX-6 and Iba-1 in normal aged F344 rats. As in the prior experiment, the majority of the OX-6 (+) cells were located in the choroid plexus stroma and, interestingly, they were Iba-1(+). These OX-6(+)Iba-1(+) cells accounted for the majority of the Iba-1(+) cells, but a small number of OX-6(+) cells were Iba-1(−). Almost all OX-6(−)Iba-1(+) cells were located outside the epithelium and had a cap-shaped appearance, reminiscent of epiplexus cells (e.g. Kolmer cells) (Figure 1B). It is worth noting that OX-6(+)Iba-1(+) cells located in the stroma, in contrast to OX-6 antigen, showed lower fluorescence intensity of Iba-1. In normal aged F344 rats, the number of OX-6(+) cells as a percentage of all choroid plexus cells was 11.0 ± 1.3%, while the percentage of OX-6(+)Iba-1(+) cells was 8.5 ± 1.7%. The percentage of OX-6(+)Iba-1(−) cells was also calculated as (total OX-6(+) cells minus OX-6(+)Iba-1(+) cells)/(all choroid plexus cells) and was 2.5 ± 0.5%, which may represent another subtype of macrophages or other immune-associated cells such as dendritic cells (Figure 1C). Overall, the OX-6(+) cells represent a large proportion of choroid plexus cells and are primarily located within the stroma. OX-6(−)Iba-1(+) cells are located outside the epithelial cells and may represent epiplexus cells based on the similarities in staining and morphology.

Minocycline mitigated iron-induced hydrocephalus and increases of OX-6(+) cells in aged rats

To determine the role of OX-6(+) cells in the development of hydrocephalus, an iron intraventricular injection model was utilized. Twenty-two aged F344 rats were divided into three groups: saline, iron and iron+minocycline. MRI scans completed at 24 hours post-injection showed that the ventricular volume of the iron group (36.0 ± 9.2 mm^3, n=8) was significantly increased compared to the saline group (11.0 ± 2.6 mm^3, n=5; $p<0.001$, Figure 2A-B). Minocycline significantly reduced ventricular dilation (21.4 ± 4.8 mm^3, n=8; $p<0.01$, Figure 2A-B).

As found in the prior experiments, almost all OX-6(+) cells were located in the choroid plexus stroma (Figure 2C). Interestingly, there was a significant increase in OX-6(+) cell number in the iron group compared to the saline group (13.8 ± 2.3% of all cells, n=8 in iron group vs. 10.2 ±1.3%, n=6 in saline group, $p<0.01$, Figure 2D). Co-injection of minocycline with iron led to reduction of OX-6(+) cells back to baseline (10.6 ± 1.2% of all cells n=8; $p<0.01$, Figure 2D). The OX-6(+)Iba-1(+) cells were also increased in the iron group compared to the saline group (11.3 ± 2.1%, n=8 in iron group vs. 7.8 ±1.2%; n=6 in saline group, $p<0.01$, Figure 2E), an effect negated by the co-administration of minocycline (9.0 ± 1.3%, n=8; $p<0.01$, Figure 2E). The OX-6(+)Iba-1(−) cells were also increased in the iron group compared to the saline group and minocycline attenuated this effect (Figure 2F). However, OX-6(+)Iba-1(−) cell number has no significant difference between these three groups.

Minocycline alleviated iron-induced hydrocephalus and increases of OX-6(+) cells in young rats

Similar to the experiments carried out with aged F344 rats, young F344 rats were randomized into the three groups and underwent intraventricular injections followed by MRI scans at 24 hours. Ventricular volume and cell numbers were calculated. Intraventricular injection of iron increased the ventricular volume (33.4 ± 15.0 mm^3, n=7) compared to saline injection (7.4 ± 6.4 mm^3, n=7; $p<0.01$, Figure 3A-B). This dilation was significantly alleviated by minocycline though not back to baseline (17.0 ± 7.4 mm^3, n=7; $p<0.05$, Figure 3A-B). The number of OX-6(+) cells as a % of all cells was again increased after iron injection (10.6 ± 1.4%, n=7) compared to saline injection (8.0 ±1.6%, n=7; $p<0.01$, Figure 3D). Though co-administration of minocycline appeared to reduce the number of OX-6(+) cells, this was not statistically significant (Figure 3D). The number of OX-6(+)Iba-1(+) cells also increased in the iron group (9.2 ± 1.6%, n=7) compared to the saline group (6.7 ±1.9%, n=7; $p<0.05$, Figure 3E). Again, though minocycline appears to reduce these effects, this was not statistically significant (Figure 3E). When comparing the OX-6(+)Iba-1(−) cell number between these three groups, OX-6(+)Iba-1(−) cells were increased in the iron group compared to the saline group without statistical difference. Meanwhile, minocycline didn't affect this population of cells apparently.

Aged rats have a higher percentage of choroid plexus stromal macrophages

Aged and young rats were compared to examine if aging affects the characteristics of stromal macrophages. When the percentage of OX-6(+) cells in the saline injection groups was compared, aged rats had more choroid plexus OX-6(+) cells (10.2 ±1.3% of all cells, n=6) than young rats (8.0 ±1.6%, n=7; $p<0.05$, Figure 4A). In the iron-injected groups, aged rats also had more OX-6(+) cells in the choroid plexus (13.8% ± 2.3%, n=8) than young rats (10.6 ± 1.4%, n=7; $p<0.05$, Figure 4B). While there was no significant difference in the total number of OX-6(+)Iba-1(+) cells between young and aged saline groups, after iron injection there was a significantly higher OX-6(+)Iba-1(+) percentage in aged rats (11.3 ±2.1%, n=8) compared to young animals (9.2 ±1.6%, n=7; $p<0.05$, Figure 4D). When comparing the percentage of OX-6(+)Iba-1(−) cells in the saline injection groups, aged rats had more OX-6(+)Iba-1(−) cells (2.4 ±0.67%, n=6) than young rats (1.2 ±0.6%, n=7; $p<0.05$, Figure 4E). In the iron-injected groups, aged rats also had more OX-6(+)Iba-1(−) cells (2.4 ± 0.8%, n=8) than young rats (1.5 ± 0.5%, n=7; $p<0.05$, Figure 4F).

Clodronate liposomes attenuated iron-induced hydrocephalus

To evaluate the effect of macrophage depletion on hydrocephalus development, clodronate liposomes were co-administered with iron injection. The ventricular volumes were decreased in the iron+clodronate group (11.6 ± 1.6 mm^3, n=5) compared with the iron+vehicle group (25.6 ± 5.1 mm^3, n=6; $p<0.001$, Figure 5A-B). The number of OX-6(+) cells (as a % of all cells) was also decreased in the iron+clodronate group (8.6 ± 0.7%, n=5) compared with the iron+vehicle group (11.1 ± 1.2%, n=6; $p<0.01$, Figure 5C-D). Unlike minocycline, clodronate liposomes failed to statistically significantly influence the number of OX-6(+)Iba-1(+) cells (Figure 5E). It, however, significantly reduced the number

of OX-6(+)Iba-1(−) cells in the iron+vehicle group (3.4 ± 1.6%, n=6) compared with the iron+clodronate group (0.9 ± 0.5%, n=5; $p<0.05$, Figure 5F).

Discussion

The choroid plexus is not only a site of the BCSFB, it is also an environment that is rich in immune cells and is now recognized as an immune organ of the brain. The immune cells present within the choroid plexus include macrophages, dendritic cells and T lymphocytes [33, 34]. Macrophages are the predominant cell type and they can be visualized with OX-6 and Iba-1 staining [11]. The data described above show that about 10% of all cells within the choroid plexus are OX-6(+). These cells are primarily located within the stroma, with a small percentage on the choroid plexus epithelium apical surface (epiplexus cells). Almost all OX-6(+) cells are also Iba-1(+) and have a morphologically elongated, dendriform or amoeboid appearance. Based on the staining pattern and morphology, OX-6(+) cells within the stroma are thought to represent choroid plexus macrophages. In this study, we divided OX-6(+) CP immune cells into two groups after iron injection. (1) OX-6(+)/Iba-1(+) cells, which are considered to be macrophages, including epiplexus macrophages and stromal macrophages. (2) OX-6(+)/Iba-1(−) cells, which are considered to be dendritic cells (DCs) but may also contain other antigen-presenting cells such as activated T cells.

Iron is a major component of erythrocytes and its release after erythrolysis plays an important role in IVH-induced brain injury and hydrocephalus [16]. Intraventricular iron injection (e.g. $FeCl_3$) itself can induce hydrocephalus [21]. In IVH-induced injury, there is evidence of the importance of toll-like receptors (TLRs), which activate the inflammatory pathways (e.g. TLR4-NFκB pathway [35, 36]). Choroid plexus inflammatory signaling can also induce CSF hypersecretion [6]. In our experiments, after intraventricular injection of iron, rats showed ventricular dilatation and an increase in OX-6(+) cells in the choroid plexus. To be more specific, macrophages (defined as OX-6(+)/Iba-1(+) cells) increased significantly after intraventricular injection of iron in both young and aged F344 rats, not DCs (defined as OX-6(+)/Iba-1(−) cells). Though a direct cause-effect relationship has not been established, this correlation may represent stromal macrophages playing a role in regulating CSF dynamics, possibly through inflammatory pathways or some other mechanism. Approximately 80% of CSF is secreted by choroid plexus epithelial cells. Choroid plexus stromal macrophages may potentially mediate inflammatory pathways within epithelial cells that can induce CSF hypersecretion[36], eventually leading to hydrocephalus. This inflammatory mechanism and resultant secondary injury may correlate clinically with post-hemorrhagic chronic hydrocephalus occurring in a delayed manner over days, rather than acutely following the initial hemorrhage.

It is possible that the increase in OX-6(+) cells at the choroid plexus after iron injection is a response to brain injury or the hydrocephalus rather than being involved in propagating those changes. We, therefore, explored the effects of trying to block the changes in the inflammatory cells and whether it would block hydrocephalus induction. Minocycline has anti-inflammatory as well as anti-apoptotic capabilities. It inhibits proteolysis immune cell activation and proliferation in several CNS disease models [37, 38]. Minocycline can also inhibit the activation of microglia/macrophages [23]. Our prior work showed

that minocycline can reduce iron overload and associated brain damage after intracerebral hemorrhage [25]. It has also been shown to alleviate hydrocephalus and a consequent increase in Iba-1(+) cells in some pathological states [18]. Other studies suggest that minocycline attenuates periventricular reactive gliosis and hydrocephalus in several animal models of hydrocephalus [23, 26]. The current study shows that minocycline can reduce ventriculomegaly caused by iron injection and that it also leads to a decrease in the percentage of OX-6(+) cells. The underlying mechanisms may be connected to the ability of minocycline to inhibit microglia/macrophage activation, alleviate neuroinflammation and chelate iron.

Clodronate liposome can selectively lead to macrophage depletion [29, 39]. This occurs by macrophage phagocytosis of liposomes and subsequent disruption of the liposome phospholipid bilayers leading to apoptosis [39]. It has been described that a single intraventricular injection of clodronate liposome can lead to complete depletion of perivascular and meningeal macrophages [31]. Other studies have demonstrated that clodronate liposome, when given intrathecally, can inhibit spinal microglial activation [40]. The data in the current study show that clodronate liposome significantly reduced the ventricular dilation caused by iron injection and reduced OX-6(+) cells. OX-6(+)/Iba-1(−) cells are probably DCs or T-cells. Those cells decreased dramatically after clodronate liposome therapy which may indicate that they have a certain degree of phagocytosis. Interestingly, however, there was no significant change in the number of OX-6(+)Iba-1(+) macrophages, leading to the speculation that other macrophage subtypes may be involved.

Age is a primary risk factor for intracerebral hemorrhage, a primary cause of adult IVH. It is, therefore, important to assess how the effects of IVH-derived iron on choroid plexus including inflammatory cells might be impacted by aging. The morphology of the choroid plexus changes with age due to irregular fibrosis of the stroma, thickening of the epithelial basement membrane and epithelial atrophy [41]. Choroid plexus function also deteriorates with age with a decline in CSF secretion and BCSFB damage [42]. A study in aged sheep suggests that normal aging alters CSF protein content, CSF secretion, and BCSFB integrity [43]. With age, immune cells of peripheral origin significantly increase in the central nervous system [44, 45]. In this study, aged rats had more choroid plexus OX-6(+)/Iba-1(+) and OX-6/Iba-1(−) cells than younger rats with similar dosing of $FeCl_3$. The data also showed that the responses tended to be greater in aged rats than young rats. This might be due to a higher number of baseline choroid plexus immune cells and the impact of aging on choroid plexus function making it more sensitive to inflammation. These findings of increased inflammation in the aged rat model may explain the known worse outcomes noted in the elderly population.

There are several limitations to this study. The first of these is that only male rats were utilized so results cannot be generalized to both sexes. Another limitation is that this study does not elucidate the mechanistic relationship between OX-6(+) cells and hydrocephalus but rather only identifies an association. Further studies will be required to understand the molecular mechanisms. That includes specifically blocking the immune response in the choroid plexus. In addition, in this proof-of-concept study, iron-induced hydrocephalus was only determined at 24 hours and intracranial pressure was not measured.

In conclusion, this study quantified the number of choroid plexus stromal macrophages, which is around 10% of all choroid plexus cells. It also reveals that ventricular volume and choroid plexus stromal macrophages increase after intraventricular injection of iron, effects which were counteracted by minocycline or clodronate liposome co-administration. Though there is a correlation between OX-6(+) cells and the hydrocephalus development, the mechanism is still unclear. It may be that inflammatory mediators from these stromal macrophages may impact BCSFB function including CSF secretion but this needs further investigation. The current data also suggest that aging increases the number of choroid plexus stromal macrophages, which may be linked to the increased susceptibility of aged rats for developing hydrocephalus.

Funding:

Y.H., R.F.K. and G.X. were supported by grants NS-096917, NS-106746, NS-112394 and NS-116786; SK was supported by NS-007222 from the National Institutes of Health.

Data Availability Statement:

Data will be available on reasonable request.

References:

1. Lun MP, Monuki ES, Lehtinen MK. Development and functions of the choroid plexus-cerebrospinal fluid system. Nat Rev Neurosci. 2015;16(8):445–57. doi: 10.1038/nrn3921. [PubMed: 26174708]
2. Kaur C, Rathnasamy G, Ling EA. The Choroid Plexus in Healthy and Diseased Brain. J Neuropathol Exp Neurol. 2016;75(3):198–213. doi: 10.1093/jnen/nlv030. [PubMed: 26888305]
3. Marques F, Sousa JC, Brito MA, Pahnke J, Santos C, Correia-Neves M, et al. The choroid plexus in health and in disease: dialogues into and out of the brain. Neurobiol Dis. 2017;107:32–40. doi: 10.1016/j.nbd.2016.08.011. [PubMed: 27546055]
4. Castro Dias M, Mapunda JA, Vladymyrov M, Engelhardt B. Structure and Junctional Complexes of Endothelial, Epithelial and Glial Brain Barriers. Int J Mol Sci. 2019;20(21). doi: 10.3390/ijms20215372.
5. Ghersi-Egea JF, Strazielle N, Catala M, Silva-Vargas V, Doetsch F, Engelhardt B. Molecular anatomy and functions of the choroidal blood-cerebrospinal fluid barrier in health and disease. Acta Neuropathol. 2018;135(3):337–61. doi: 10.1007/s00401-018-1807-1. [PubMed: 29368213]
6. Karimy JK, Reeves BC, Damisah E, Duy PQ, Antwi P, David W, et al. Inflammation in acquired hydrocephalus: pathogenic mechanisms and therapeutic targets. Nat Rev Neurol. 2020;16(5):285–96. doi: 10.1038/s41582-020-0321-y. [PubMed: 32152460]
7. McMenamin PG, Wealthall RJ, Deverall M, Cooper SJ, Griffin B. Macrophages and dendritic cells in the rat meninges and choroid plexus: three-dimensional localisation by environmental scanning electron microscopy and confocal microscopy. Cell Tissue Res. 2003;313(3):259–69. doi: 10.1007/s00441-003-0779-0. [PubMed: 12920643]
8. Ling EA, Kaur C, Lu J. Origin, nature, and some functional considerations of intraventricular macrophages, with special reference to the epiplexus cells. Microscopy research and technique. 1998;41(1):43–56. doi: 10.1002/(SICI)1097-0029(19980401)41:1<43::AID-JEMT5>3.0.CO;2-V. [PubMed: 9550136]
9. Mundt S, Mrdjen D, Utz SG, Greter M, Schreiner B, Becher B. Conventional DCs sample and present myelin antigens in the healthy CNS and allow parenchymal T cell entry to initiate neuroinflammation. Sci Immunol. 2019;4(31). doi: 10.1126/sciimmunol.aau8380.
10. Dando SJ, Kazanis R, Chinnery HR, McMenamin PG. Regional and functional heterogeneity of antigen presenting cells in the mouse brain and meninges. Glia. 2019;67(5):935–49. doi: 10.1002/glia.23581. [PubMed: 30585356]

11. Rodriguez-Lorenzo S, Konings J, van der Pol S, Kamermans A, Amor S, van Horssen J, et al. Inflammation of the choroid plexus in progressive multiple sclerosis: accumulation of granulocytes and T cells. Acta Neuropathol Commun. 2020;8(1):9. doi: 10.1186/s40478-020-0885-1. [PubMed: 32014066]
12. Bosche B, Mergenthaler P, Doeppner TR, Hescheler J, Molcanyi M. Complex Clearance Mechanisms After Intraventricular Hemorrhage and rt-PA Treatment-a Review on Clinical Trials. Transl Stroke Res. 2020;11(3):337–44. doi: 10.1007/s12975-019-00735-6. [PubMed: 31522408]
13. Hanley DF. Intraventricular hemorrhage: severity factor and treatment target in spontaneous intracerebral hemorrhage. Stroke. 2009;40(4):1533–8. doi: STROKEAHA.108.535419 [pii]10.1161/STROKEAHA.108.535419. [PubMed: 19246695]
14. Hemorrhagic Stroke Academia Industry Roundtable P. Basic and Translational Research in Intracerebral Hemorrhage: Limitations, Priorities, and Recommendations. Stroke. 2018;49(5):1308–14. doi: 10.1161/STROKEAHA.117.019539. [PubMed: 29618555]
15. Keep RF, Hua Y, Xi G. Intracerebral haemorrhage: mechanisms of injury and therapeutic targets. Lancet Neurology. 2012;11(8):720–31. doi: 10.1016/S1474-4422(12)70104-7. [PubMed: 22698888]
16. Chen Z, Gao C, Hua Y, Keep RF, Muraszko K, Xi G. Role of iron in brain injury after intraventricular hemorrhage. Stroke. 2011;42(2):465–70. doi: STROKEAHA.110.602755 [pii] 10.1161/STROKEAHA.110.602755. [PubMed: 21164132]
17. Garton T, Hua Y, Xiang J, Xi G, Keep RF. Challenges for intraventricular hemorrhage research and emerging therapeutic targets. Expert Opin Ther Targets. 2017;21(12):1111–22. doi: 10.1080/14728222.2017.1397628. [PubMed: 29067856]
18. Gu C, Hao X, Li J, Hua Y, Keep RF, Xi G. Effects of minocycline on epiplexus macrophage activation, choroid plexus injury and hydrocephalus development in spontaneous hypertensive rats. J Cereb Blood Flow Metab. 2019;39(10):1936–48. doi: 10.1177/0271678X19836117. [PubMed: 30862302]
19. Okubo S, Strahle J, Keep RF, Hua Y, Xi G. Subarachnoid hemorrhage-induced hydrocephalus in rats. Stroke. 2013;44(2):547–50. doi: 10.1161/STROKEAHA.112.662312. [PubMed: 23212164]
20. Strahle JM, Garton T, Bazzi AA, Kilaru H, Garton HJ, Maher CO, et al. Role of hemoglobin and iron in hydrocephalus after neonatal intraventricular hemorrhage. Neurosurgery. 2014;75(6):696–705; discussion 6. doi: 10.1227/NEU.0000000000000524. [PubMed: 25121790]
21. Gao C, Du H, Hua Y, Keep RF, Strahle J, Xi G. Role of red blood cell lysis and iron in hydrocephalus after intraventricular hemorrhage. J Cereb Blood Flow Metab. 2014;34(6):1070–5. doi: 10.1038/jcbfm.2014.56. [PubMed: 24667910]
22. Meng H, Li F, Hu R, Yuan Y, Gong G, Hu S, et al. Deferoxamine alleviates chronic hydrocephalus after intraventricular hemorrhage through iron chelation and Wnt1/Wnt3a inhibition. Brain Res. 2015;1602:44–52. doi: 10.1016/j.brainres.2014.08.039. [PubMed: 25152462]
23. Xu H, Tan G, Zhang S, Zhu H, Liu F, Huang C, et al. Minocycline reduces reactive gliosis in the rat model of hydrocephalus. BMC Neurosci. 2012;13:148. doi: 10.1186/1471-2202-13-148. [PubMed: 23217034]
24. Machado LS, Sazonova IY, Kozak A, Wiley DC, El-Remessy AB, Ergul A, et al. Minocycline and tissue-type plasminogen activator for stroke: assessment of interaction potential. Stroke. 2009;40(9):3028–33. doi: STROKEAHA.109.556852 [pii] 10.1161/STROKEAHA.109.556852. [PubMed: 19628804]
25. Cao S, Hua Y, Keep RF, Chaudhary N, Xi G. Minocycline Effects on Intracerebral Hemorrhage-Induced Iron Overload in Aged Rats: Brain Iron Quantification With Magnetic Resonance Imaging. Stroke. 2018;49(4):995–1002. doi: 10.1161/STROKEAHA.117.019860. [PubMed: 29511126]
26. McAllister JP 2nd, Miller JM. Minocycline inhibits glial proliferation in the H-Tx rat model of congenital hydrocephalus. Cerebrospinal Fluid Res. 2010;7:7. doi: 10.1186/1743-8454-7-7. [PubMed: 20507614]
27. Yang Y, Zhang K, Yin X, Lei X, Chen X, Wang J, et al. Quantitative Iron Neuroimaging Can Be Used to Assess the Effects of Minocycline in an Intracerebral Hemorrhage Minipig Model. Transl Stroke Res. 2020;11(3):503–16. doi: 10.1007/s12975-019-00739-2. [PubMed: 31696415]

28. van Rooijen N, Sanders A. Elimination, blocking, and activation of macrophages: three of a kind? J Leukoc Biol. 1997;62(6):702–9. doi: 10.1002/jlb.62.6.702. [PubMed: 9400810]
29. Jing C, Bian L, Wang M, Keep RF, Xi G, Hua Y. Enhancement of Hematoma Clearance With CD47 Blocking Antibody in Experimental Intracerebral Hemorrhage. Stroke. 2019;50(6):1539–47. doi: 10.1161/STROKEAHA.118.024578. [PubMed: 31084334]
30. Wei J, Wang M, Jing C, Keep RF, Hua Y, Xi G. Multinucleated Giant Cells in Experimental Intracerebral Hemorrhage. Transl Stroke Res. 2020;11(5):1095–102. doi: 10.1007/s12975-020-00790-4. [PubMed: 32090277]
31. Polfliet MM, Goede PH, van Kesteren-Hendrikx EM, van Rooijen N, Dijkstra CD, van den Berg TK. A method for the selective depletion of perivascular and meningeal macrophages in the central nervous system. J Neuroimmunol. 2001;116(2):188–95. [PubMed: 11438173]
32. Zhang J, Novakovic N, Hua Y, Keep RF, Xi G. Role of lipocalin-2 in extracellular peroxiredoxin 2-induced brain swelling, inflammation and neuronal death. Exp Neurol. 2021;335:113521. doi: 10.1016/j.expneurol.2020.113521. [PubMed: 33129840]
33. Ransohoff RM, Engelhardt B. The anatomical and cellular basis of immune surveillance in the central nervous system. Nat Rev Immunol. 2012;12(9):623–35. doi: 10.1038/nri3265. [PubMed: 22903150]
34. Wan Y, Gao F, Ye F, Yang W, Hua Y, Keep RF, et al. Effects of aging on hydrocephalus after intraventricular hemorrhage. Fluids Barriers CNS. 2020;17(1):8. doi: 10.1186/s12987-020-0169-y. [PubMed: 32106865]
35. Rivest S Molecular insights on the cerebral innate immune system. Brain Behav Immun. 2003;17(1):13–9. doi: 10.1016/s0889-1591(02)00055-7. [PubMed: 12615045]
36. Karimy JK, Zhang J, Kurland DB, Theriault BC, Duran D, Stokum JA, et al. Inflammation-dependent cerebrospinal fluid hypersecretion by the choroid plexus epithelium in posthemorrhagic hydrocephalus. Nat Med. 2017;23(8):997–1003. doi: 10.1038/nm.4361. [PubMed: 28692063]
37. Yenari MA, Xu L, Tang XN, Qiao Y, Giffard RG. Microglia potentiate damage to blood-brain barrier constituents: improvement by minocycline in vivo and in vitro. Stroke. 2006;37(4):1087–93. doi: 01.STR.0000206281.77178.ac [pii] 10.1161/01.STR.0000206281.77178.ac. [PubMed: 16497985]
38. Tikka TM, Koistinaho JE. Minocycline provides neuroprotection against N-methyl-D-aspartate neurotoxicity by inhibiting microglia. J Immunol. 2001;166(12):7527–33. doi: 10.4049/jimmunol.166.12.7527. [PubMed: 11390507]
39. Van Rooijen N, Sanders A. Liposome mediated depletion of macrophages: mechanism of action, preparation of liposomes and applications. J Immunol Methods. 1994;174(1-2):83–93. doi: 10.1016/0022-1759(94)90012-4. [PubMed: 8083541]
40. Wang YR, Mao XF, Wu HY, Wang YX. Liposome-encapsulated clodronate specifically depletes spinal microglia and reduces initial neuropathic pain. Biochem Biophys Res Commun. 2018;499(3):499–505. doi: 10.1016/j.bbrc.2018.03.177. [PubMed: 29596830]
41. Serot JM, Foliguet B, Bene MC, Faure GC. Choroid plexus and ageing in rats: a morphometric and ultrastructural study. Eur J Neurosci. 2001;14(5):794–8. doi: 10.1046/j.0953-816x.2001.01693.x. [PubMed: 11576183]
42. Preston JE. Ageing choroid plexus-cerebrospinal fluid system. Microsc Res Tech. 2001;52(1):31–7. doi: 10.1002/1097-0029(20010101)52:1<31::AID-JEMT5>3.0.CO;2-T. [PubMed: 11135446]
43. Chen RL, Kassem NA, Redzic ZB, Chen CP, Segal MB, Preston JE. Age-related changes in choroid plexus and blood-cerebrospinal fluid barrier function in the sheep. Exp Gerontol. 2009;44(4):289–96. doi: 10.1016/j.exger.2008.12.004. [PubMed: 19133323]
44. Honarpisheh P, Blixt FW, Blasco Conesa MP, Won W, d'Aigle J, Munshi Y, et al. Peripherally-sourced myeloid antigen presenting cells increase with advanced aging. Brain Behav Immun. 2020. doi: 10.1016/j.bbi.2020.08.023.
45. Kaunzner UW, Miller MM, Gottfried-Blackmore A, Gal-Toth J, Felger JC, McEwen BS, et al. Accumulation of resident and peripheral dendritic cells in the aging CNS. Neurobiol Aging. 2012;33(4):681–93 e1. doi: 10.1016/j.neurobiolaging.2010.06.007. [PubMed: 20692074]

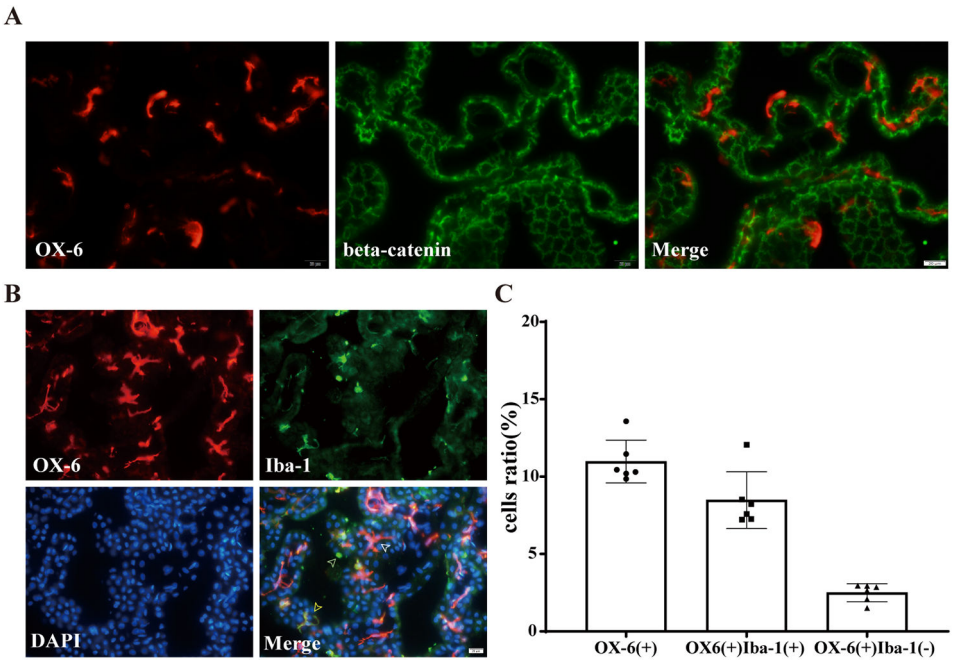

Figure 1. Baseline characteristics of choroid plexus stromal macrophages in aged rats.

(A) Immunofluorescence double-staining of OX-6 and beta-catenin in choroid plexus of normal aged F344 rat. Note the presence of many OX-6 positive cells within the choroid plexus stroma (below the epithelium). (B) Immunofluorescence double-staining of OX-6 and Iba-1 in choroid plexus of normal aged F344 rat. White arrow shows OX-6(+)Iba-1(−) cells, green arrow shows OX-6(−)Iba-1(+) cells, yellow arrow shows OX-6(+)Iba-1(+) cells. (C) The number of OX-6(+) cells, OX-6(+)Iba-1(+) cells and OX-6(+)Iba-1(−) cells as a percentage of the total number of choroid plexus cells. Values are mean ± SD, n=6.

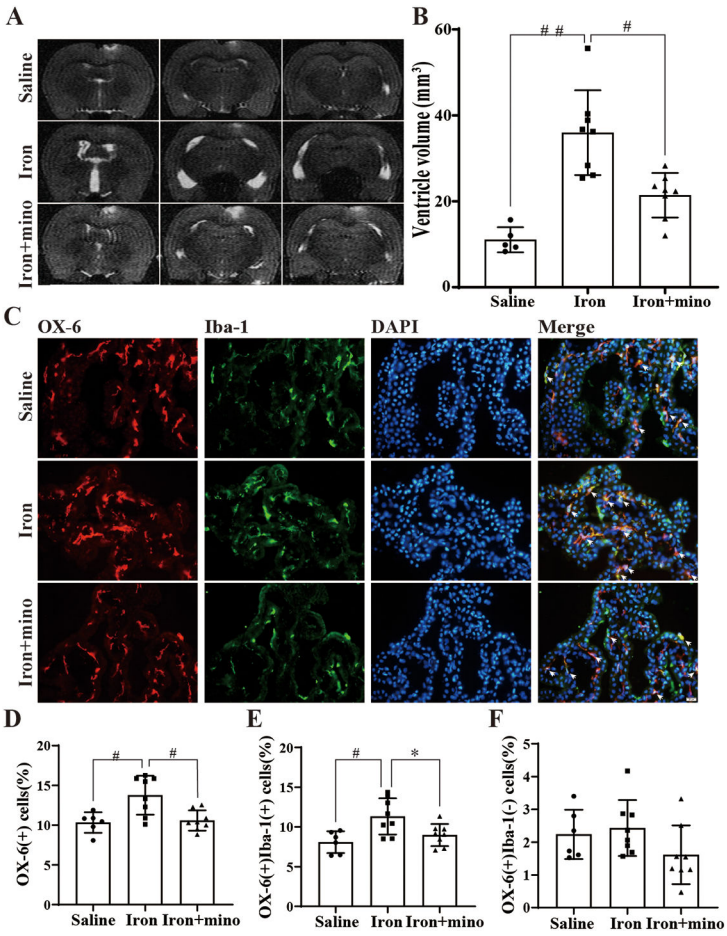

Figure 2. Intraventricular iron injection increases ventricular volume and the number of OX-6(+) in aged rats, effects mitigated by minocycline.

(A) Examples of T2-weighted MRI scans at 24 hours after intraventricular injection of saline, iron ($FeCl_3$) or iron ($FeCl_3$) + minocycline (mino) in aged F344 rats. Note the dilated ventricles in the iron-injected rats. (B) Quantification of ventricular volume. Values are mean ± SD, n=5 in saline group, n=8 in iron group and n=8 in iron+mino group. $p<0.001$ when comparing the three groups by one-way ANOVA-test, ##$p<0.001$ for iron vs. saline group and #$p<0.01$ for iron vs. iron+mino group by Tukey's multiple comparisons test. (C) Immunofluorescence double-staining of choroid plexus OX-6 and Iba-1 in saline, iron and iron+mino group at 24 hours. White arrows show OX-6(+)Iba-1(+) co-labeled cells. (D) The number of OX-6(+) cells was calculated as a percentage of the total number of choroid plexus cells. Values are mean ± SD, n=6 in saline group, n=8 in iron group and n=8 in iron+mino group. $p<0.05$ when comparing the three groups by one-way ANOVA-test, #$p<0.01$ for iron vs. saline group and #$p<0.01$ for iron vs. iron+mino group by Tukey's multiple comparisons test. (E) The percentage of OX-6(+)Iba-1(+) cells were calculated relative to the total number of choroid plexus cells. Values are mean ± SD, n=6 in saline group, n=8 in iron group and n=8 in iron+mino group. $p<0.01$ when comparing the three groups by one-way ANOVA-test, #$p<0.01$ for iron vs. saline group and *$p<0.05$ for iron vs. iron+mino group by Tukey's multiple comparisons test. (F) The percentage of OX-6(+)Iba-1(−) cells were calculated relative to the total number of choroid plexus cells.

Values are mean ± SD, n=6 in saline group, n=8 in iron group and n=8 in iron+mino group. P>0.05 when comparing the three groups by one-way ANOVA-test.

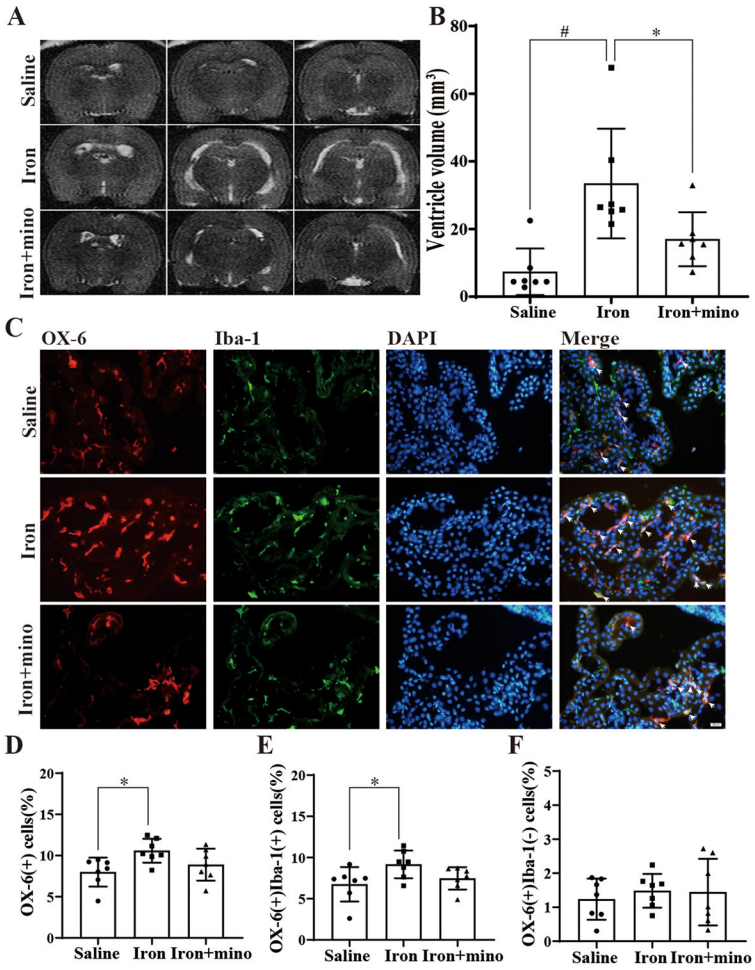

Figure 3. Intraventricular iron injection increases ventricular volume and the number of OX-6(+) in young rats, effects mitigated by minocycline.

(A) Examples of T2-weighted MRI scans at 24 hours after intraventricular injection of saline, iron ($FeCl_3$) or iron ($FeCl_3$) + minocycline (mino) in young F344 rats. (B) Quantification of ventricular volume. Values are mean ± SD, n=7 in saline, n=7 in iron and n=7 in iron+mino groups. $p<0.01$ comparing the three groups by one-way ANOVA-test, #$p<0.01$ for iron vs. saline group and *$p<0.05$ for iron vs. iron+mino group by Tukey's multiple comparisons test. (C) Immunofluorescence double-staining of choroid plexus OX-6 and Iba-1 in saline, iron and iron+mino groups at 24 hours. White arrows show OX-6(+)Iba-1(+) co-labeled cells. (D) The number of OX-6(+) cells was calculated as a % of the total number of choroid plexus cells. Values are mean ± SD, n=7 in saline, n=7 in iron and n=7 in iron+mino groups. $p<0.05$ comparing the three groups by one-way ANOVA-test, *$p<0.05$ for iron vs. saline group by Tukey's multiple comparisons test. (E) The percentage of OX-6(+)Iba-1(+) cells were calculated relative to the total number of choroid plexus cells. Values are mean ± SD, n=7 in saline, n=7 in iron and n=7 in iron+mino groups. $p<0.05$ when comparing the three groups by one-way ANOVA-test, *$p<0.05$ for iron vs. saline group by Tukey's multiple comparisons test. (F) The percentage of OX-6(+)Iba-1(−) cells were calculated relative to the total number of choroid plexus cells. Values are mean ± SD,

n=7 in saline, n=7 in iron and n=7 in iron+mino groups. P>0.05 when comparing the three groups by one-way ANOVA-test.

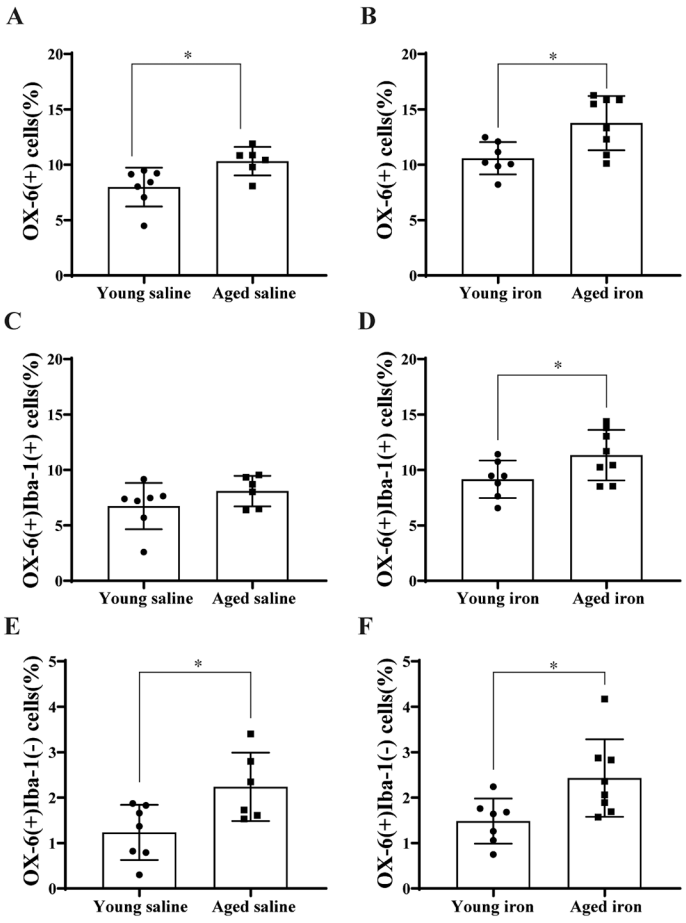

Figure 4. Aged rats have more OX-6(+) cells than young rats.

(A) Comparison of the number of OX-6(+) cells (expressed as a % of total choroid plexus cells) in young and aged saline groups. Aged saline group n=6, young saline group, n=7. *p<0.05 by t-test. (B) Comparison of the percentage of OX-6(+) cells between young and aged iron groups. Aged iron group n=8, young iron group, n=7. *p<0.05 by t-test. (C) Comparison of the percentage of OX-6(+)Iba-1(+) cells between young and aged saline groups. Aged saline group n=6, young saline group n=7. p>0.05 by t-test. (D) Comparison of the percentage of OX-6(+)Iba-1(+) cells between young and aged iron groups. Aged iron group n=8, young iron group, n=7. *p<0.05 by t-test. Values are mean ± SD. (E) Comparison of the percentage of OX-6(+)Iba-1(−) cells between young and aged saline groups. Aged saline group n=6, young saline group n=7. *p<0.05 by t-test. (F) Comparison of the percentage of OX-6(+)Iba-1(−) cells between young and aged iron groups. Aged iron group n=8, young iron group, n=7. *p<0.05 by t-test. Values are mean ± SD.

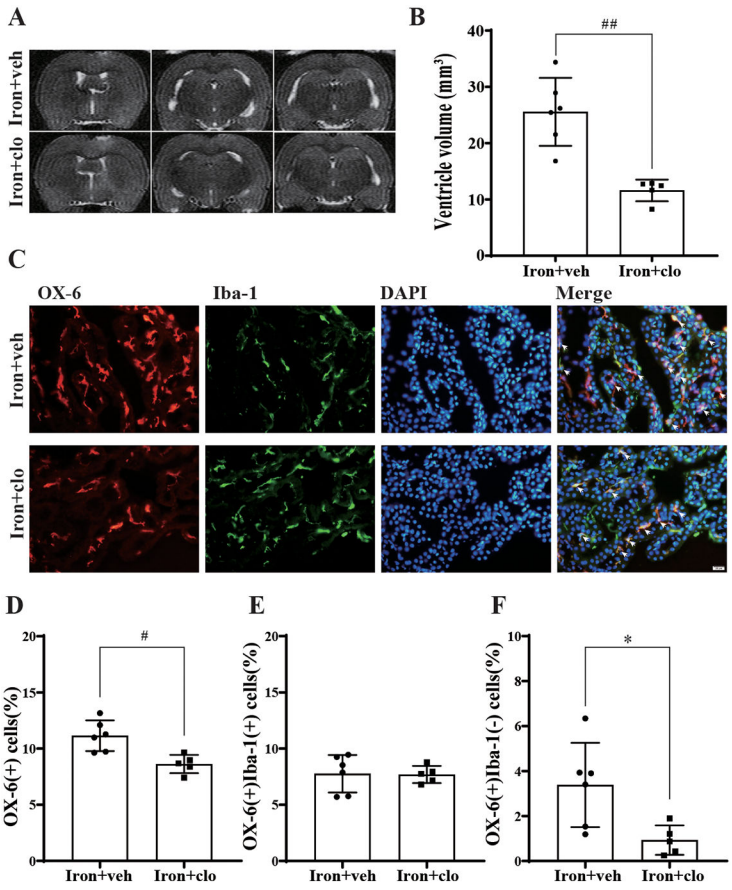

Figure 5:

(A) Examples of T2-weighted MRI scans at 24 hours after intraventricular injection of iron ($FeCl_3$) + control liposome (veh) or iron ($FeCl_3$) + clodronate liposome (clo) in young F344 rats. (B) Quantification of ventricular volume. Values are mean ± SD, n=6 in iron+veh group, n=5 in iron+clo group. ##p<0.001 by t-test. (C) Immunofluorescence double-staining of choroid plexus OX-6 and Iba-1 in iron+veh and iron+clo groups at 24 hours. White arrows show OX-6(+)Iba-1(+) co-labeled cells. (D) The number of OX-6(+) cells as a percentage of the total number of choroid plexus cells. Values are mean ± SD, n=6 in iron+veh group, n=5 in iron+clo group. #p<0.01 by t-test. (E) The percentage of OX-6(+)Iba-1(+) cells were calculated relative to the total number of choroid plexus cells. Values are mean ± SD, n=6 in iron+veh group, n=5 in iron+clo group. p>0.05 by t-test. (F) The percentage of OX-6(+)Iba-1(−) cells were calculated relative to the total number of choroid plexus cells. Values are mean ± SD, n=6 in iron+veh group, n=5 in iron+clo group. *p<0.05 by t-test.